Physics Letters A 172 (1993) 247–255
North-Holland

PHYSICS LETTERS A

Lyapunov exponents and return maps for a model of a laser with saturable absorber

A. Zeni, J.A.C. Gallas
Laboratório de Óptica Quântica da UFSC, 88040-900 Florianópolis, Brazil and Instituto de Física da UFRGS, 91540-000 Porto Alegre, Brazil

A. Fioretti [1], F. Papoff, B. Zambon and E. Arimondo
Dipartimento di Fisica, Università di Pisa, Pisa, Italy

Received 30 July 1992; revised manuscript received 16 October 1992; accepted for publication 20 October 1992
Communicated by A.R. Bishop

Maximum Lyapunov exponents and return maps are derived from a numerical integration of equations describing a laser with intracavity saturable absorber. Different sets of parameters are used in the models. It is shown that deterministic chaos with a small positive Lyapunov exponent is associated to multibranched return time return maps while noisy evolution leads to maps with a lattice structure.

1. Introduction

The laser with intracavity saturable absorber (LSA) is a high sensitivity quantum optical system useful for laser spectroscopy investigations, but presenting also a complex non-linear dynamical behaviour. The chaotic behaviour of the single-mode operation of LSA has been investigated in different experimental configurations based on an infrared CO_2 laser containing a molecular absorber [1–4], and analysed numerically in different models [5–7] and more recently through a comparison with one-dimensional maps [8] and through a topological approach [9]. On the basis of those different methods, the LSA time dependence has been classified as chaotic, and associated with the presence of a homoclinic orbit to a saddle cycle. On the contrary, the straight approach of verifying the presence of chaos through a calculation of Lyapunov exponents has been applied only in a few cases mainly for models not corresponding specifically to the experimental observations [5,10]. It is the main purpose of this paper to present Lyapunov exponents calculated for a model that has been previously applied to interpret experimental observations. A key feature of the chaotic behaviour presented by the infrared CO_2 LSA is the vibrational structure of the CO_2 amplifier medium. Even though most LSA models take into account the vibrational structure, they differ in the description of the rotational structure of the absorber medium. In this paper the maximum Lyapunov exponent is derived for several sets of control parameters on the basis of a LSA model [6] specifically tested through a comparison with experiments [7].

The return map approach has been used as a very convenient tool for the classification of LSA regimes [8]. In this paper return maps are derived from time-dependent numerical solutions of the LSA equations, for the same set of parameters used in the determination of the Lyapunov exponents. The theoretical return maps allow us to make a comparison with the experimental ones reported in ref. [8], and to conclude that also the experimentally observed time dependences are associated to positive Lyapunov exponents, i.e. they are chaotic. Finally the comparison with the topological approach, presented in ref. [9], allows us to discuss some characteristic features of the return maps associated to a

[1] Also at Scuola Normale Superiore, Pisa, Italy.

homoclinic orbit to a saddle cycle via phase-space Poincaré sections. As an important result of the present work, we confirm that the LSA experimental chaotic sequences for which the topological analysis has been applied, correspond to a case of a small positive Lyapunov exponent. If a system has an unstable orbit of low period, according to the classification introduced in ref. [9], with a small positive Lyapunov exponent, an evolution near the unstable periodic orbit, with close return to its previous evolution, takes place. The organisation of such orbits and the identification of the topological invariants allow one to determine the presence of a strange attractor [11].

2. LSA model and Lyapunov exponents

For a two-level laser with adiabatic elimination of the polarization, the relevant variables are the electric field E, or intensity $I \propto E^2$, and the population difference D between the lower and the upper level. For infrared CO_2 lasers operating on excited vibrational transitions, a third variable is required to describe the population in the other states [2], and through a proper transformation the equation for the third variable S assumes a very simple form [6]. For the absorber medium the population difference $\bar{D}$ between the resonant levels is the only required variable. Thus the LSA is modelled by the following set of equations,

$$\frac{dE}{dt} = -\tfrac{1}{2}(-AD+\bar{A}\bar{D}+1)E+\zeta(t)\,, \tag{1a}$$

$$\frac{dD}{dt} = \gamma(1-D-DE^2)-c_1(D-S)\,, \tag{1b}$$

$$\frac{dS}{dt} = -\gamma_1(S-D)\,, \tag{1c}$$

$$\frac{d\bar{D}}{dt} = -\bar{\gamma}(\bar{D}-1+a\bar{D}E^2)\,, \tag{1d}$$

where the electric field E has been normalised to the amplifier saturation value and the time t is normalised to the cavity decay rate k, A and $\bar{A}$ are respectively the small signal amplification and absorption constants, also normalised to the cavity decay rate, and D and $\bar{D}$ are normalised to 1. The vibrational relaxation rates of amplifier and absorber, γ and $\bar{\gamma}$, are also normalised to the cavity decay rate. Finally the parameter a is the ratio between the saturation values of the amplifier and the absorber. In eq. (1a) the term ζ is a Gaussian white noise, defined by the relation $\langle \zeta(t)\zeta(t') \rangle = 2Q\delta(t-t')$ representing the spontaneous emission source required to start laser action.

If an adiabatic elimination of the $\bar{D}$ variable is performed, the main features of the LSA chaotic behaviour remain in the reduced three-equation model [6]. In the present analysis use will be made mainly of the full model, because for parameter values relevant to the experimental investigation the adiabatic elimination of $\bar{D}$ cannot always be applied. For the first two sets of parameters of table 1, we used directly the equation for the evolution of the laser intensity instead of eq. (1a) for the electric field amplitude, without the noise term, which turns out to be not relevant for these parameter values.

We have investigated the LSA behaviour for the three sets of parameters listed in table 1. The first set of parameters is taken from the theoretical analysis of ref. [6], and corresponds to a non-periodic irregular time dependence of the laser intensity, which was assigned as chaotic in that analysis. Figure 1a shows the temporal evolution of the laser intensity I, as derived from numerical integration of eqs. (1) using a standard fourth-order Runge–Kutta integrator with constant step $h=0.025$. The time depen-

Table 1
Parameter values and initial conditions for the three numerical simulations. The parameter values explore different chaotic scenarios so as to reproduce the experimental observations.

Parameter	Set I	Set II	Set III
A	27.0	44.0	5.7
$\bar{A}$	0.78	1.0	1.1
a	0.3	0.25948	10.0
γ	0.0016	0.0008	0.0016
c_1	0.1	0.099	0.1
γ_1	0.1	0.0998	0.1
$\bar{\gamma}$	1.2	0.0769	–
$E(0)$	$42^{1/2}$	$42^{1/2}$	42
$D(0)$	1/43	1/43	1/43
$S(0)$	1/43	1/43	1/43
$\bar{D}(0)$	1/9.5	1/9.5	–

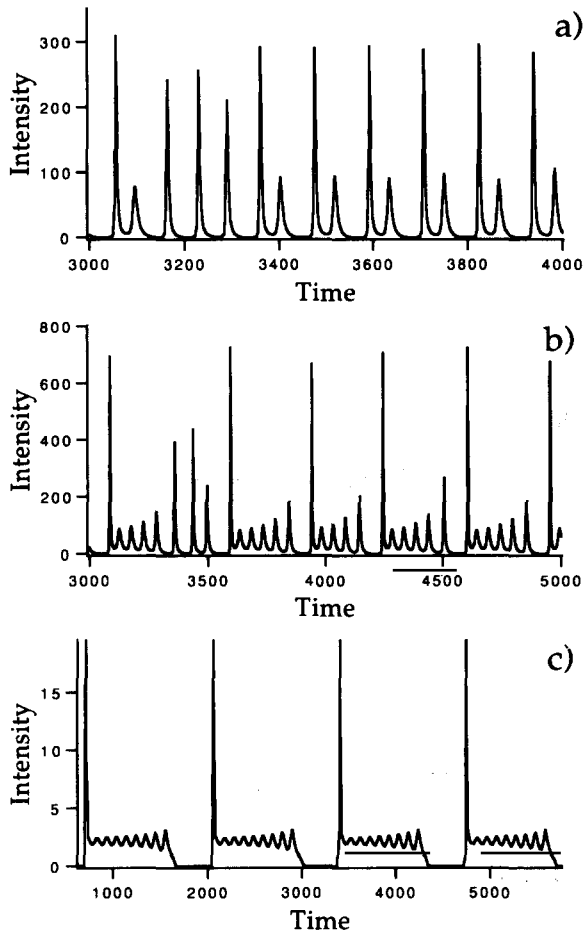

Fig. 1. Time dependence of the LSA laser intensity I, measured in units of the amplifier saturation intensity: (a) for the parameter set I of table 1, (b) for the parameter set II, (c) for the parameter set III. Time is measured in units of the cavity decay time, with $t=0$ the starting time for integration.

dence is classified as hesitation between $P^{(0)}$ and $P^{(1)}$ pulses [4], i.e. an unpredictable sequence of pulses with one large peak and pulses with one large peak followed by a small one.

By numerically integrating eqs. (1a)–(1d) for a time up to 8.0×10^4, a very large set of data has been derived. The maximum Lyapunov exponent λ_{max} has been computed as described in ref. [12]. However the norm was recalculated at each step of the integration, following the requirements of Shimada and Nagashima [13]. The result for the λ_{max} calculation is reported in fig. 2 as a function of the data set contained in an integration time t_{int}. It appears from this figure that the value of λ_{max} is positive and clearly stabilises to a value of 0.006, in units of k, when the largest data set is used.

The second set of parameters derives from the analysis presented in ref. [4] for the interpretation of experimental results. The time dependence for this parameter set, shown in fig. 1b, is classified as hesitation between $P^{(4)}$ and $P^{(5)}$ regimes. Thus the second parameter set corresponds to nearly the central region, assigned as chaotic, in the phase diagram of ref. [4]. Also for this parameter set the maximum Lyapunov exponent, determined as described above, turns out to be positive and converges to 0.005.

The third set of parameters of table 1, here included mainly to have a complete comparison between Lyapunov exponents and return time return maps, has been also investigated in ref. [6] for evolution in the (E, D, S) phase space and location in the phase diagram. In this case an adiabatic elimination of the $\bar{D}$ variable was applied and a three-equation set was numerically integrated. The time evolution of the laser intensity, reported in fig. 1c, appears not very different from those obtained for other sets of laser parameters. The main difference is that the presence of spontaneous emission noise in the laser equation (1) is essential to produce an unpredictable evolution of the laser intensity. In absence of spontaneous emission the time evolution is periodic, while for increasing values of the noise intensity, it becomes irregular; in particular, for $Q=1.75\times10^{-7}$ the laser intensity time evolution appears as a mixing of $P^{(8)}$ and $P^{(9)}$ pulses. This behaviour of the numerical solutions leads to a comparison with similar experimental regimes and is important for the identification of the presence or not of deterministic chaos. In effect the question of evolution associated either to homoclinic chaos or to noise presence has been crucial for instance in the characterisation of the Belusov–Zhabotinskii reaction [14]. Our derivation of the maximum Lyapunov exponent, $\lambda=-2.16\times10^{-6}$ for the evolution without noise and $\lambda=-1.87\times10^{-5}$ for the evolution in the presence of the noise level specified above, confirms the interpretation in terms of a deterministic non-chaotic dynamics whose irregularity is governed by noise [6]. Moreover, the occurrence of a negative Lyapunov exponent and the comparison of corre-

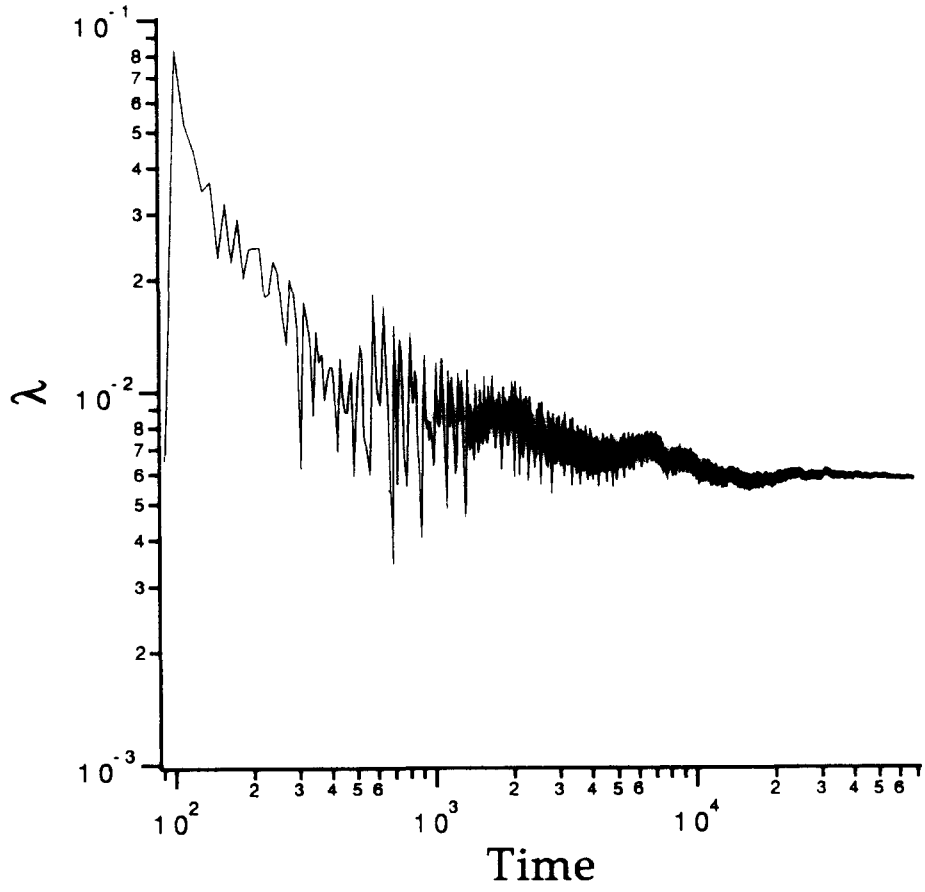

Fig. 2. Maximum LSA Lyapunov exponent versus integration time, with 0.025 integration step, for parameter set I of table 1.

sponding return time return maps, will prove that experimental and theoretical return maps with a lattice structure are not associated to deterministic chaos.

3. Return maps

The derivation of one-dimensional return maps from experimental time series data and their comparison with theoretical ones, are important steps towards the characterisation of a system's dynamics [8].

We have applied the derivation of return maps also to the theoretical time series for the laser intensity. One-dimensional intensity return maps (I_i, I_{i+1}) may be derived from an embedding space built up using the usual time delay technique. Return time return maps (RTRMs) are much simpler to derive from time series data, because they do not require the reconstruction of the embedding space. The RTRM is related to an intensity return map through a function associating to each point on the Poincaré section of the embedding space a corresponding return time [8]. If that function is monotone, hence invertible, a one to one correspondence between intensity and return time maps exists. In order to derive a RTRM from the numerical data for the laser intensity, a section with $I=\text{const}$ was introduced into the time series of the laser intensity. All the time intervals t_i between successive points with equal laser intensity I and same sign of $\mathrm{d}I/\mathrm{d}t$ were determined. The $(t_i,$

t_{i+1}) return map of fig. 3a reports each time interval versus the previous one for the first data set of table 1, using a section plane I=const that intersects all the peaks in the time dependent laser intensity.

The map of fig. 3a presents one branch with positive slope and two branches with negative slope con-

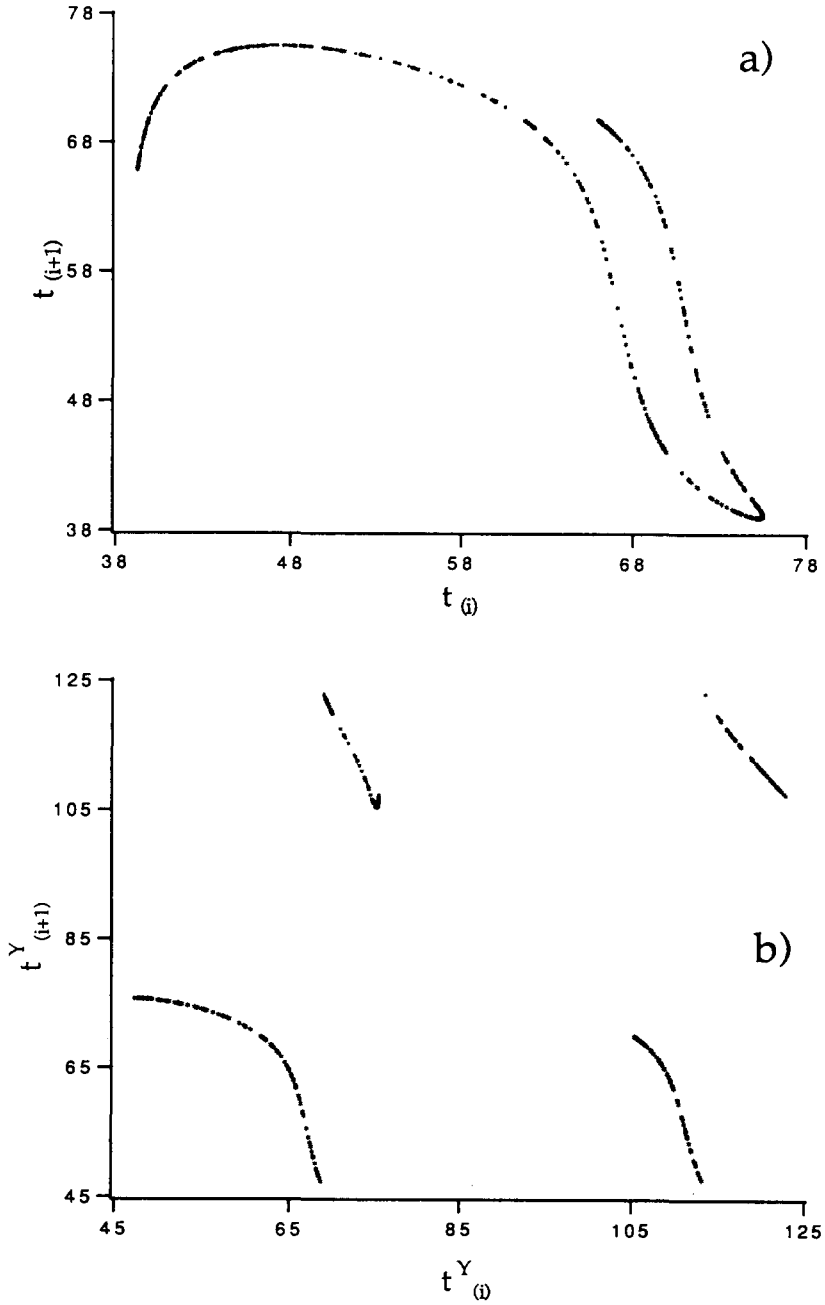

Fig. 3. (a) The complete return time return map with a I=50 section on the time series, as derived from the parameter set I. (b) Return time return map as derived from the negative slope parts of the complete map in (a).

nected at their minimum and lying one above the other. The positive slope branch corresponds to the small peaks while the two negative slope branches are originated by the large peaks in the time dependent laser intensity of fig. 3a. Those large peaks come from the re-injection mechanism; there are two negative slope branches, one above the other, because the function which associates points on the Poincaré section with return times is multivalued, as discussed in ref. [8]. We have coded the small peaks on the positive slope branch with x and the large peaks on the negative slope branch with y. We point out that within each branch there is no spreading of the points in the transverse direction so that the motion of the system can really be described by a 1-D map.

For comparison, the experimental LSA data of ref. [8] give rise to 1-D return maps with only two branches, one for the small peaks and one for the large ones, which correspond, respectively, to an orientation reversing and an orientation preserving manifold on the LSA Smale horseshoe induced template [9]. Moreover, the LSA experimental maps show that, in most cases, the application leading from the Poincaré section to the RTRM, is single valued. In the case of fig. 3a instead, the presence of the two branches means that part of the large peaks lie on an orientation preserving manifold and that the induced template could be larger than those derived in ref. [9]. A more detailed study of this problem is now in progress.

A return map (t_i^y, t_{i+1}^y) for return times, derived from the full one of fig. 3a considering orbits leaving and returning only on the negative slope branches, is reported in fig. 3b. The return map of fig. 3b may equivalently be obtained if the $I=$const section cuts only those peaks with larger laser intensity.

Maps as in fig. 3 have been observed in the LSA experiments and also derived theoretically assuming that the LSA evolution is originated by stable and unstable manifolds to a limit cycle, while approaching a quadratic tangency [8]. The maps of fig. 3 have been derived from the LSA equations for a set of parameters corresponding to a positive Lyapunov exponent. Thus the present analysis demonstrates that the experimentally observed LSA signals with multibranched maps as in fig. 3 correspond to a weakly diverging chaotic evolution.

When the RTRM analysis is applied to the second set of parameters, i.e. the time dependent laser intensity of fig. 1b, the maps of figs. 4a and 4b are obtained. Figure 4a reports the full RTRM, while fig. 4b reports the restricted return time maps associated to the negative slope parts of fig. 4a. The map of fig. 4a presents two branches with positive slope and two with negative slope. Each branch is very well resolved, with no spreading of the points in the transverse direction. The whole map suggests a complex folding of the unstable manifold so it cannot be compared in a simple way with the usual theoretical 1-D maps studied in ref. [8]. Maps as in fig. 4b have also been observed in the LSA experiment, however their analysis in terms of quadratic tangency was not performed. This numerical simulation confirms that also those complicated experimental multibranched maps are expressions of a chaotic evolution, even if they are associated with orbits of more complex symbolic name.

For the third set of table 1, the RTRM for a $I=10$ Poincaré section is shown in fig. 5. It must be compared to the maps of figs. 3b and 4b because it is equivalent to a map restricted to the negative slope part. In effect, a complete RTRM could not be performed in this case due to the presence of very small oscillations of the intensity that could not be resolved. It presents a characteristic lattice-like structure. The same lattice-like structure has been observed in all the maps relative to LSA experiments with an SF_6 gas absorber and in those relative to some experiments with an OsO_4 absorber [15]. The present analysis, with the determination of a negative Lyapunov exponent for the corresponding time evolution, confirms the identification of the experimental observations with a dynamics of the system governed by noise.

4. Conclusions

The calculation of the maximum Lyapunov exponent and return maps for the LSA intensity from a theoretical time series has allowed a comparison with experimental results and an identification of experimental observations as chaotic or noise controlled. The positive Lyapunov exponent turns out to be very small, around $(5-6)\times 10^{-3}$ in units of the cavity decay rate, corresponding to a weakly diverg-

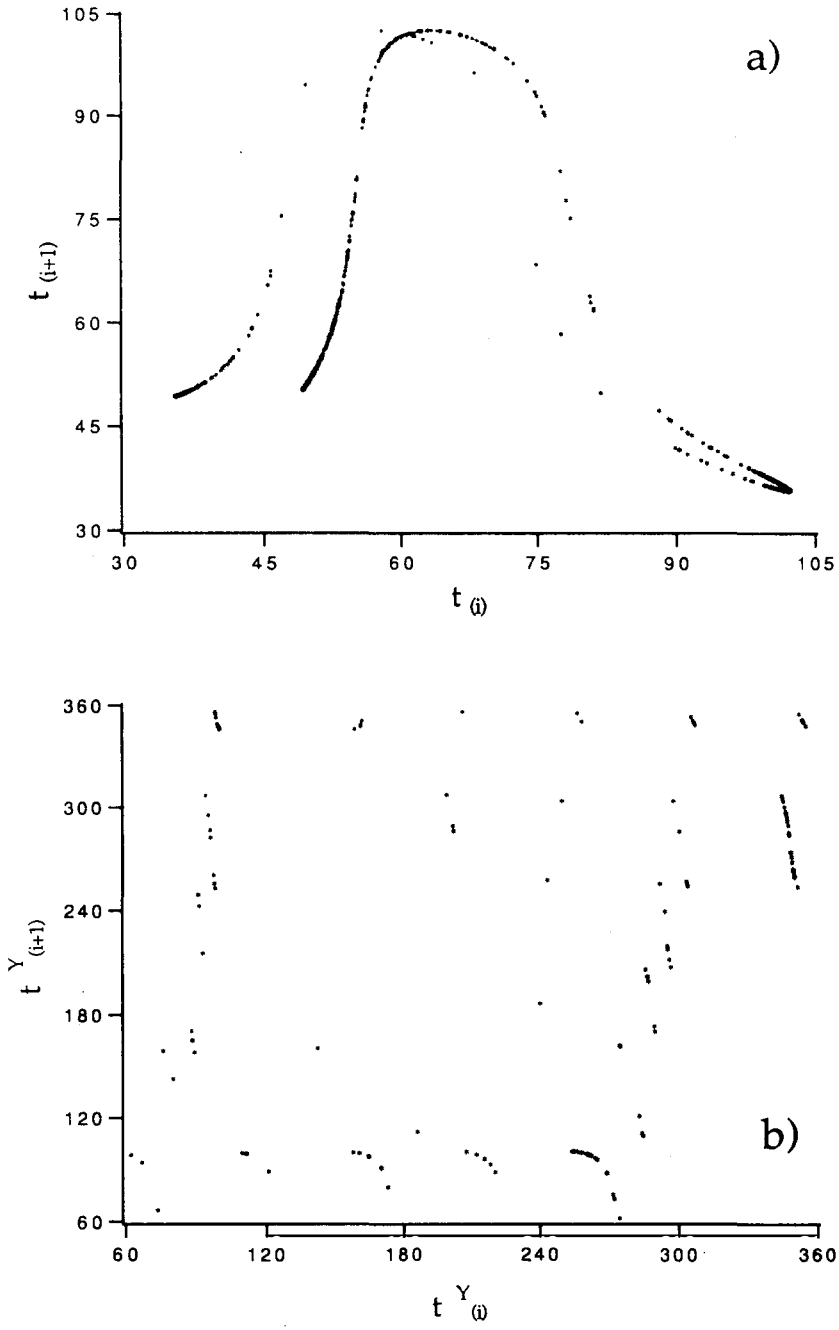

Fig. 4. (a) And (b) as in fig. 3 for the parameter set II using a $I=50$ section on the time series.

ing chaotic dynamics. It is interesting to notice that similar very low values of the positive Lyapunov exponent have been derived also in the theoretical analysis of an LSA model contained in ref. [10].

The two main objectives of this work are (i) to confirm that the LSA model leads to return maps

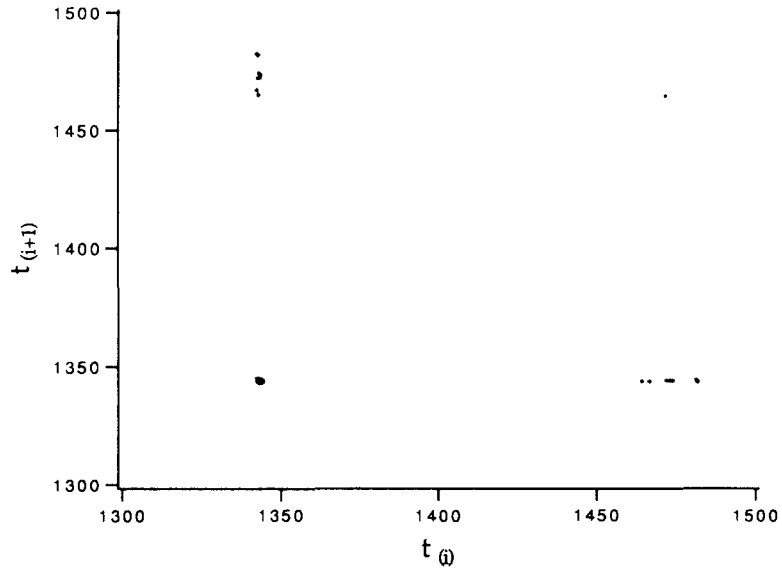

Fig. 5. Return time return map, as in figs. 3b and 4b, obtained for the parameter set III using a $I=10$ section on the time series.

analogous to those observed in the experiment, and (ii) to show that the multibranched and lattice-like return maps correspond to deterministic chaos and noise driven evolution, respectively. Both objectives have been realized. However, for what concerns the second one, it could have been suggested to determine the Lyapunov exponent directly from experimental data in order to comment about chaoticity. In effect, new approaches have been recently developed to derive the Lyapunov exponent from short time series data [16]. This direct approach will be also performed, however it should be remarked that, by deriving this maximal exponent from the model, we obtained the result that LSA chaos is characterized by a very small positive Lyapunov exponent, differing from zero only by 0.5% of the characteristic rate of the system. The determination of such a small exponent from experimental data using the approach quoted above should be checked carefully.

The resulting Lyapunov exponents of the present analysis are important also for similar experimental observations, for instance those on a plasma discharge of ref. [17]. In conclusion, as RTRMs are easily derived from experimental data, maps containing approximately 200–300 points and presenting a characteristic multibranched or lattice-like structure allow a direct identification of either deterministic chaos with small positive Lyapunov exponent or noise controlled evolution.

Acknowledgement

The present work was initiated during a one month stay of one of us (EA) in Florianópolis. We thank the Conselho Nacional de Pesquisa (CNPq), Brazil, for supporting this visit. JACG is a Senior Research Fellow of the CNPq. This work was partially supported by Consorzio INFM-Italy and by EEC under contract No. SC1*-CT91-0679 (TSTS).

References

[1] D. Hennequin, F. de Tomasi, B. Zambon and E. Arimondo, Phys. Rev. A 37 (1988) 2243.
[2] M. Tachikawa, F.L. Hong, K. Tani and T. Shimizu, Phys. Rev. Lett. 60 (1988) 2266; 61 (1988) 1042.
[3] D. Dangoisse, A. Bekkali, F. Papoff and P. Glorieux, Europhys. Lett. 6 (1988) 335.
[4] F. de Tomasi, D. Hennequin, B. Zambon and E. Arimondo, J. Opt. Soc. Am. B 6 (1989) 45.
[5] M. Lefranc, D. Dangoisse and D. Hennequin, J. Opt. Soc. Am. B 8 (1991) 239.

[6] B. Zambon, Phys. Rev. A 44 (1991) 688; in: OSA Proc. on Nonlinear dynamics in optical systems, Vol. 7, eds. N.B. Abraham, E.M. Garmire and P. Mandel (Optical Society of America, Washington, DC, 1991) p. 512.
[7] B. Zambon, F. de Tomasi, D. Hennequin and E. Arimondo, Phys. Rev. A 40 (1988) 3782.
[8] F. Papoff, A. Fioretti and E. Arimondo, Phys. Rev. A 44 (1991) 4639.
[9] F. Papoff, A. Fioretti, E. Arimondo, G.B. Midlin, H.G. Solari and R. Gilmore, Phys. Rev. Lett. 68 (1992) 1128.
[10] T. Tohei, M. Tachikawa and T. Shimizu, Phys. Rev. A 45 (1992) 5166.
[11] G.B. Midlin, H.G. Solari, M.A. Natiello, R. Gilmore and X.J. Hou, J. Nonlinear Sci. 1 (1991) 147.
[12] G. Contopoulos, L. Galgani and A. Giorgilli, Phys. Rev. A 18 (1978) 1183.
[13] I. Shimada and T. Nagashima, Prog. Theor. Phys. 61 (1979) 1605.
[14] F. Argoul, A. Arneodo and P. Richetti, J. Chim. Phys. 84 (1987) 1367.
[15] A. Fioretti, F. Papoff, B. Zambon and E. Arimondo, in: OSA Proc. on Nonlinear dynamics in optical systems, Vol. 7, eds. N.B. Abraham, E.M. Garmire and P. Mandel (Optical Society of America, Washington, DC, 1991) p. 554.
[16] X. Zeng, R. Eykholt and R.A. Pielke, Phys. Rev. Lett. 66 (1991) 3229, and references therein.
[17] T. Braun, J.A. Lisboa and J.A.C. Gallas, Phys. Rev. Lett. 68 (1992) 2270.